

IMPLICIT-EXPLICIT METHODS FOR TIME-DEPENDENT PARTIAL DIFFERENTIAL EQUATIONS*

URI M. ASCHER[†], STEVEN J. RUUTH[‡], AND BRIAN T.R. WETTON[§]

Abstract. Implicit-explicit (IMEX) schemes have been widely used, especially in conjunction with spectral methods, for the time integration of spatially discretized partial differential equations (PDEs) of diffusion-convection type. Typically, an implicit scheme is used for the diffusion term and an explicit scheme is used for the convection term. Reaction-diffusion problems can also be approximated in this manner. In this work we systematically analyze the performance of such schemes, propose improved new schemes, and pay particular attention to their relative performance in the context of fast multigrid algorithms and of aliasing reduction for spectral methods.

For the prototype linear advection-diffusion equation, a stability analysis for first-, second-, third-, and fourth-order multistep IMEX schemes is performed. Stable schemes permitting large time steps for a wide variety of problems and yielding appropriate decay of high frequency error modes are identified. Numerical experiments demonstrate that weak decay of high frequency modes can lead to extra iterations on the finest grid when using multigrid computations with finite difference spatial discretization, and to aliasing when using spectral collocation for spatial discretization. When this behavior occurs, use of weakly damping schemes such as the popular combination of Crank–Nicolson with second-order Adams–Bashforth is discouraged and better alternatives are proposed.

Our findings are demonstrated on several examples.

Key words. method of lines, finite differences, spectral methods, aliasing, multigrid, stability region

AMS subject classifications. 65J15, 65M20

1. Introduction. Various methods have been proposed to integrate dynamical systems arising from spatially discretized time-dependent partial differential equations (PDEs). For problems with terms of different types, implicit-explicit (IMEX) schemes have been often used, especially in conjunction with spectral methods [7], [16]. For convection-diffusion problems, for example, one would use an explicit scheme for the convection term and an implicit scheme for the diffusion term. Reaction-diffusion problems can also be approximated in this manner. In this work we systematically analyze the performance of such schemes, propose improved new schemes, and pay particular attention to their relative performance in the context of fast multigrid algorithms and of aliasing reduction for spectral methods.

Consider a time-dependent PDE in which the spatial derivatives have been discretized by central finite differences or by some spectral method. This gives rise to a large system of ordinary differential equations (ODEs) in time which typically has the form

$$(1) \quad \dot{u} = f(u) + \nu g(u)$$

where $\|g\|$ is normalized and ν is a nonnegative parameter. The term $f(u)$ in (1) is some possibly nonlinear term which we do not want to integrate implicitly. This could

* Received by the editors June 1, 1993; accepted for publication December 20, 1993.

[†] Department of Computer Science, University of British Columbia, Vancouver, British Columbia, V6T 1Z4, Canada (ascher@cs.ubc.ca). The research of this author was partially supported by the Natural Sciences and Engineering Research Council of British Columbia grant OGP0004306.

[‡] Department of Mathematics, University of British Columbia, Vancouver, British Columbia, V6T 1Z2, Canada (ruuth@math.ubc.ca). The research of this author was partially supported by the Natural Sciences and Engineering Research Council of British Columbia postgraduate scholarship.

[§] Department of Mathematics, University of British Columbia, Vancouver, British Columbia, V6T 1Z2, Canada (wetton@math.ubc.ca). The research of this author was partially supported under Natural Sciences and Engineering Research Council of British Columbia grant OGP0122105.

be because the Jacobian of $f(u)$ is nonsymmetric and nondefinite and an iterative solution of the implicit equations is desired, or the Jacobian could be dense, as in spectral methods, requiring the inversion of a full matrix at each time step. One may simply wish to integrate $f(u)$ explicitly for ease of implementation. The term $\nu g(u)$, however, is a stiff term which should be integrated implicitly to avoid excessively small time steps. Frequently $\nu g(u)$ is a linear diffusion term, in which case the implicit equations form a linear system which is positive definite, symmetric, and sparse. Such systems can be solved efficiently by iterative techniques (e.g., [26], [11]). Thus, for problems of the form (1) it often makes sense to integrate $\nu g(u)$ implicitly and $f(u)$ explicitly, yielding an IMEX scheme.

The most popular IMEX scheme hitherto has been a combination of second-order Adams–Bashforth for the explicit (“convection”) term and Crank–Nicolson for the implicit (“diffusion”) term [16], [7], [1]. Applied to (1) this gives

$$(2) \quad \frac{u^{n+1} - u^n}{k} = \frac{3}{2}f(u^n) - \frac{1}{2}f(u^{n-1}) + \frac{\nu}{2}[g(u^{n+1}) + g(u^n)]$$

where k is the constant discretization step size and u^n is the numerical approximation to $u(kn)$. Other IMEX methods have also been considered, e.g., [18], [25], [15].

A wide variety of other applications for IMEX schemes are also possible. For example, solutions to reaction-diffusion systems arising in chemistry and mathematical biology can be computed using this technique. For these problems the nonlinear reaction term can be treated explicitly while the diffusion term is treated implicitly. Examples of reaction-diffusion systems from a biological standpoint can be found in [19]. We report about these in a separate paper [21].

Several authors have analyzed specific IMEX schemes. For example, an experimental analysis of several IMEX schemes including (2) was carried out in [2]. Some stability properties for certain second-order IMEX schemes were determined in [25]. The schemes (17) and (24) below were considered in a Navier–Stokes context in [15]. These studies do not address how to choose the best IMEX scheme for a given system (1).

In this paper, we seek efficient IMEX schemes for convection-diffusion-type problems using a systematic approach. First we derive, in §2, classes of linear multistep IMEX schemes. Classes of s -step schemes turn out to have optimal order s and to depend on s parameters.

We then restrict our attention in §3 to a prototype advection-diffusion equation in one dimension

$$(3) \quad U_t = aU_x + \nu U_{xx}$$

where a and ν are constants, $\nu > 0$, subject to periodic boundary conditions. A von Neumann analysis (see, e.g., [23]) can then be applied, yielding in effect a safe diagonalization of (1) and allowing us to consider a scalar test equation

$$(4) \quad \dot{x} = (\alpha + i\beta)x$$

as is customary for ODEs (see, e.g., [12]) for values of α, β on an ellipse. An analysis of IMEX schemes for (4) is then performed, seeking methods which allow the largest stable time steps. In particular, for $\nu \gg 1$ we seek methods possessing a mild time step restriction since the system (1) is dominated by the implicitly handled “diffusion term.” For other values of $\nu \geq 0$ we seek schemes which have reasonable time-stepping restrictions, e.g., comparable to the Courant–Friedrichs–Lewy (CFL) condition [23].

In §4 we perform a variety of numerical experiments using finite difference and pseudospectral methods on linear and nonlinear problems of convection-diffusion type in one and two spatial dimensions. These experiments agree with the theory of §3. Furthermore, we discuss and demonstrate the use of IMEX schemes which yield strong decay of high frequency spatial modes. This property has important implications for the efficiency of time-dependent multigrid methods and of pseudospectral methods. An appropriate IMEX scheme (but not the popular (2)!) can reduce aliasing in pseudospectral methods. In the multigrid context, similar methods can reduce the number of multigrid cycles needed per time step, in effect acting as smoothers (cf. [14], [10]).

Conclusions and recommendations are summarized in §5. Perhaps the most surprising conclusion is that the most popular IMEX scheme (2) can essentially always be outperformed by other IMEX schemes. Moreover, a modification of (2) is almost always at least as good as (2) and at times much better.

2. General linear multistep IMEX schemes. We now derive s -step IMEX schemes for (1), $s \geq 1$. Letting k be the discretization step size and u^n denote the approximate solution at $t_n = kn$, we may write these schemes as

$$(5) \quad \frac{1}{k} u^{n+1} + \frac{1}{k} \sum_{j=0}^{s-1} a_j u^{n-j} = \sum_{j=0}^{s-1} b_j f(u^{n-j}) + \nu \sum_{j=-1}^{s-1} c_j g(u^{n-j})$$

where $c_{-1} \neq 0$. See [8] for some stability and convergence results. For a smooth function $u(t)$, expand (5) in a Taylor series about $t_n = n\Delta t$ to obtain the truncation error. This yields

$$(6) \quad \begin{aligned} & \frac{1}{k} \left[1 + \sum_{j=0}^{s-1} a_j \right] u(t_n) + \left[1 - \sum_{j=1}^{s-1} j a_j \right] \dot{u}(t_n) + \cdots + \frac{k^{p-1}}{p!} \left[1 + \sum_{j=1}^{s-1} (-j)^p a_j \right] u^{(p)}(t_n) \\ & - \sum_{j=0}^{s-1} b_j f(u(t_n)) + k \sum_{j=1}^{s-1} j b_j \left. \frac{df}{dt} \right|_{t=t_n} - \cdots - \frac{k^{p-1}}{(p-1)!} \sum_{j=1}^{s-1} (-j)^{p-1} b_j \left. \frac{d^{p-1}f}{dt^{p-1}} \right|_{t=t_n} \\ & - \nu \sum_{j=-1}^{s-1} c_j g(u(t_n)) - k\nu \left[c_{-1} - \sum_{j=-1}^{s-1} c_j \right] \left. \frac{dg}{dt} \right|_{t=t_n} - \cdots \\ & - \frac{k^{p-1}}{(p-1)!} \nu \left[c_{-1} + \sum_{j=1}^{s-1} c_j (-j)^{p-1} \right] \left. \frac{d^{p-1}g}{dt^{p-1}} \right|_{t=t_n} + \mathcal{O}(k^p). \end{aligned}$$

Applying (1) to the truncation error (6), an order p scheme is obtained provided

$$(7) \quad \begin{aligned} & 1 + \sum_{j=0}^{s-1} a_j = 0, \\ & 1 - \sum_{j=1}^{s-1} j a_j = \sum_{j=0}^{s-1} b_j = \sum_{j=-1}^{s-1} c_j, \\ & \frac{1}{2} + \sum_{j=1}^{s-1} \frac{j^2}{2} a_j = - \sum_{j=1}^{s-1} j b_j = c_{-1} - \sum_{j=1}^{s-1} j c_j, \end{aligned}$$

$$\frac{1}{p!} + \sum_{j=1}^{s-1} \frac{(-j)^p}{p!} a_j = \sum_{j=1}^{s-1} \frac{(-j)^{p-1} b_j}{(p-1)!} = \frac{c_{-1}}{(p-1)!} + \sum_{j=1}^{s-1} \frac{(-j)^{p-1} c_j}{(p-1)!}.$$

It is not difficult to prove the following theorem [22].

THEOREM 2.1. *For the s -step IMEX scheme (5), the following hold.*

- (a) *The $2p + 1$ constraints of the system (7) are linearly independent, provided $p \leq s$. Thus, there exist s -step IMEX schemes of order s .*
- (b) *An s -step IMEX scheme cannot have order of accuracy greater than s .*
- (c) *The family of s -step IMEX schemes of order s has s parameters.*

We thus restrict all further discussion to s -step IMEX schemes of order s .

3. Analysis for a test advection-diffusion problem. For the prototype problem (3), using the standard second-order centred approximations D_1 and D_2 for the first and second derivatives, respectively, we obtain the corresponding semidiscrete equations

$$\dot{U}_i = aD_1U_i + \nu D_2U_i, \quad 1 \leq i \leq M.$$

(Here, a uniform spatial grid with M points has been employed.) Applying a discrete Fourier transform diagonalizes this system to

$$\dot{x}_j = i\beta_j x_j + \alpha_j x_j, \quad j = 1, \dots, M$$

where α_j and β_j are given by

$$(8) \quad (\alpha_j, \beta_j) = \left(\frac{2\nu}{h^2} [\cos(2\pi jh) - 1], \frac{a}{h} \sin(2\pi jh) \right).$$

For notational convenience, we write

$$(9) \quad \dot{x} = i\beta x + \alpha x.$$

We then consider values (α, β) which lie on the ellipse of Fig. 1. Note that the solution of (9) decays in time,

$$|x(t_{n+1})| = e^{\alpha k} |x(t_n)|.$$

Applying the general multistep IMEX scheme (5) to (9) yields

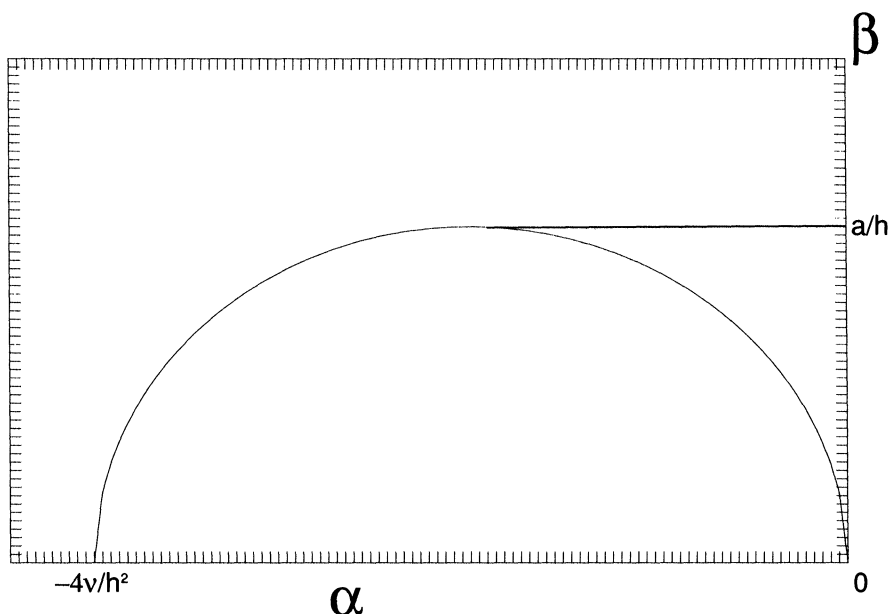
$$(10) \quad \frac{1}{k} x^{n+1} + \frac{1}{k} \sum_{j=0}^{s-1} a_j x^{n-j} = \sum_{j=0}^{s-1} b_j i\beta x^{n-j} + \sum_{j=-1}^{s-1} c_j \alpha x^{n-j},$$

which is a linear difference equation with constant coefficients. (When comparing (10) to (5) note that ν is buried in α .) The solutions of the difference equation (10) are of the form

$$x^{n+1} = p_1 \tau_1^n + p_2 \tau_2^n + \dots + p_s \tau_s^n$$

where τ_j is the j th root of the characteristic equation defined by

$$(11) \quad \Phi(z) \equiv (1 - c_{-1}\alpha k)z^s + \sum_{j=0}^{s-1} (a_j - b_j i\beta k - c_j \alpha k) z^{s-j-1}$$


 FIG. 1. Half ellipse of possible (α, β) .

and p_j is constant for τ_j simple and a polynomial in n otherwise. Clearly, stability holds for $|\tau_j| \leq 1$, τ_j simple, and $|\tau_j| < 1$ where τ_j is a multiple root.

Remark. Below we will be interested in the entire range of $\nu \geq 0$. For the purely hyperbolic case $\nu = 0$, our choice of the centered difference D_1 then leaves out the important characteristic-based methods. However, it is well known that a one-sided scheme can be interpreted as a centred scheme plus an artificial diffusion term (e.g., [13]), so we do want to pay close attention to $\nu = \mathcal{O}(h)$. \square

3.1. First-order IMEX schemes. The one-parameter family of first-order IMEX schemes for (1) can be written as

$$(12) \quad u^{n+1} - u^n = kf(u^n) + \nu k[(1 - \gamma)g(u^n) + \gamma g(u^{n+1})]$$

and we restrict $0 \leq \gamma \leq 1$ to prevent large truncation error.

The choice $\gamma = 0$ yields the forward Euler scheme

$$u^{n+1} - u^n = kf(u^n) + \nu kg(u^n).$$

This scheme is fully explicit, and will not be considered further. The choice $\gamma = \frac{1}{2}$ yields the second-order Crank–Nicolson scheme when $f = 0$. Another possibility is to apply backward Euler to g and forward Euler to f . This choice ($\gamma = 1$) yields

$$(13) \quad u^{n+1} - u^n = kf(u^n) + \nu kg(u^{n+1}).$$

IMEX schemes such as (13) which apply a backward differentiation formula (BDF) discretization [9] to g and which extrapolate f to time step $(n + 1)$ will be referred to as semiimplicit BDF (SBDF) schemes.

Applied to the test equation (4), the general IMEX scheme (5) gives

$$x^{n+1} = \xi(\alpha, \beta)x^n, \quad \text{where } \xi(\alpha, \beta) = \frac{1 + k\alpha(1 - \gamma) + ik\beta}{1 - k\gamma\alpha}.$$

The stability region is thus $\{(\alpha, \beta) : |\xi(\alpha, \beta)| \leq 1\}$.

Note that these one-step schemes trivially accommodate variable time-stepping and use relatively little storage. The choice $\gamma = 1$ is particularly attractive because strong decay occurs for α large and negative. However, first-order IMEX schemes have the shortcoming that they are unstable near the nonzero β -axis (i.e., for ν sufficiently small and $a \neq 0$ fixed but arbitrary) since

$$|\xi(0, \beta)| = |1 + ik\beta| = \sqrt{1 + k^2\beta^2} > 1.$$

Furthermore, at least a second-order time-stepping scheme is often desirable since a second-order spatial discretization is used. We thus consider higher-order methods for the remainder of this paper.

3.2. Second-order IMEX schemes. Approximating (1) to second order using IMEX schemes leaves two free parameters. If we center our schemes in time about time step $(n + \gamma)$ to second order, we obtain the following family:

$$(14) \quad \frac{1}{k} \left[\left(\gamma + \frac{1}{2} \right) u^{n+1} - 2\gamma u^n + \left(\gamma - \frac{1}{2} \right) u^{n-1} \right] = (\gamma + 1)f(u^n) - \gamma f(u^{n-1}) \\ + \nu \left[\left(\gamma + \frac{c}{2} \right) g(u^{n+1}) + (1 - \gamma - c)g(u^n) + \frac{c}{2}g(u^{n-1}) \right].$$

Some of these methods are quite familiar. For example, selecting $(\gamma, c) = (\frac{1}{2}, 0)$ yields the popular scheme (2),

$$\frac{1}{k}[u^{n+1} - u^n] = \frac{3}{2}f(u^n) - \frac{1}{2}f(u^{n-1}) + \frac{\nu}{2}[g(u^{n+1}) + g(u^n)].$$

Because it applies Crank–Nicolson for the implicit part and second-order Adams–Bashforth for the explicit part, this scheme will be referred to as CNAB (Crank–Nicolson, Adams–Bashforth). Below, we show that the best asymptotic decay properties for $\gamma = \frac{1}{2}$ occur when $c = \frac{1}{8}$. This choice gives

$$(15) \quad \frac{1}{k}[u^{n+1} - u^n] = \frac{3}{2}f(u^n) - \frac{1}{2}f(u^{n-1}) + \nu \left[\frac{9}{16}g(u^{n+1}) + \frac{3}{8}g(u^n) + \frac{1}{16}g(u^{n-1}) \right].$$

Because of the obvious similarity to CNAB, this scheme will be called modified CNAB (MCNAB). Note that in comparison to CNAB, MCNAB does require the additional evaluation or storage of $g(u^{n-1})$.

By setting $(\gamma, c) = (0, 1)$ in (14) we obtain another method which has been applied to spectral applications (e.g., [4])

$$(16) \quad \frac{1}{2k}[u^{n+1} - u^{n-1}] = f(u^n) + \frac{\nu}{2}[g(u^{n+1}) + g(u^{n-1})].$$

This scheme uses leap frog explicitly and something similar to Crank–Nicolson implicitly (cf. [17]). For this reason, this method shall be referred to as CNLF (Crank–Nicolson, leap frog).

Finally, setting $(\gamma, c) = (1, 0)$ yields

$$(17) \quad \frac{1}{2k}[3u^{n+1} - 4u^n + u^{n-1}] = 2f(u^n) - f(u^{n-1}) + \nu g(u^{n+1})$$

which shall be referred to as SBDF since this scheme is centered about time step $(n + 1)$. Other authors, e.g. [25], call this scheme extrapolated Gear.

Having determined integration formulae, we direct our attention to obtaining stability properties for second-order IMEX schemes. The second-degree characteristic polynomial resulting from (14) applied to $\dot{x} = (\alpha + i\beta)x$ is given by

$$(18) \quad \Phi(z) = \left[\gamma + \frac{1}{2} - \alpha k \left(\gamma + \frac{c}{2} \right) \right] z^2 - [2\gamma + i\beta k(\gamma + 1) + \alpha k(1 - \gamma - c)]z + \gamma - \frac{1}{2} + i\beta k\gamma - \alpha k\frac{c}{2}.$$

It is easy to verify that at the origin $(\alpha, \beta) = (0, 0)$ the roots of Φ are 1 and $\frac{2\gamma-1}{2\gamma+1}$. Thus, all of these schemes are stable at the origin, provided $\nu \geq 0$.

Because the parameter c in (18) is always multiplied by α we choose c according to stability properties for $|\alpha| \gg \frac{1}{k}$. For this case, the roots of the characteristic equation (18) are given approximately by

$$\left(\gamma + \frac{c}{2} \right) \tau^2 + (1 - \gamma - c)\tau + \frac{c}{2} = 0$$

which yields

$$\tau_{1,2} = \frac{\gamma + c - 1 \pm \sqrt{(1 - \gamma)^2 - 2c}}{2\gamma + c}.$$

For any (γ, c) , evaluating

$$(19) \quad \mathcal{D}_{\gamma,c} \equiv \max(|\tau_1|, |\tau_2|)$$

provides an estimate of the high frequency modal decay for large ν . Minimization over c determines the method with the strongest asymptotic high frequency decay for a particular γ . This yields (see [22])

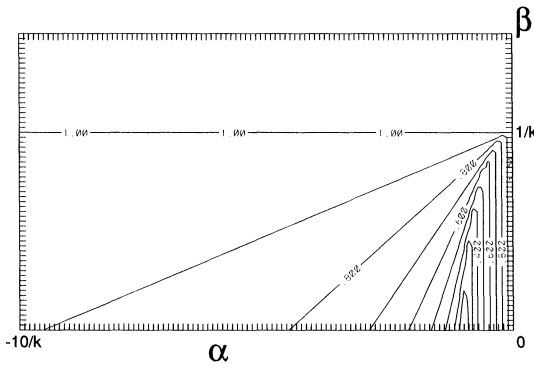
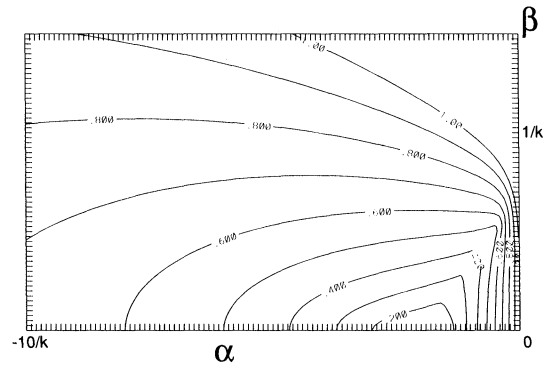
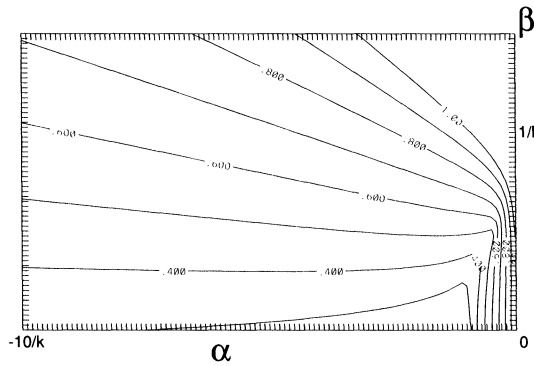
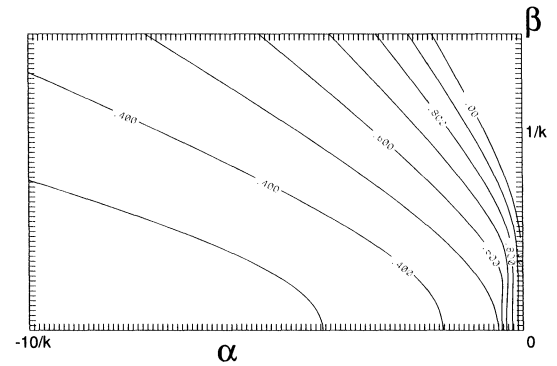
$$(20) \quad c = \frac{(1 - \gamma)^2}{2} \quad \text{for } \gamma > 0, \\ c \geq \frac{1}{2} \quad \text{for } \gamma = 0.$$

The choice

$$(21) \quad c = 1 - \gamma$$

also proves useful (see [22]). The schemes SBDF, MCNAB, and CNLF satisfy (20), the schemes SBDF and CNLF satisfy (21), but CNAB satisfies neither. Also, minimization of (19) over γ and c determines that the SBDF scheme (17) possesses the strongest asymptotic decay of second-order methods.

Further information can be obtained from the stability contours in the $\alpha - \beta$ plane. These plots are displayed in Figs. 2–5. Figure 2 shows the contours for CNLF. This method is stable for all $\nu \geq 0$, provided $k < \frac{h}{a}$. Such a time step restriction is

FIG. 2. *Stability contours for CNLF.*FIG. 3. *Stability contours for CNAB.*FIG. 4. *Stability contours for MCNAB.*FIG. 5. *Stability contours for SBDF.*

undesirable since it applies even for large ν and small h . Furthermore, the decay of high frequency modes can be weak, tending to 1 as $\alpha \rightarrow -\infty$. Comparison of CNLF to other second-order methods such that $\gamma = 0$ suggests that CNLF produces the largest stability region among such methods.

The contours for CNAB are plotted in Fig. 3. This method has a reasonable time step restriction for larger ν and small h . It is unstable near the β -axis, however. It also suffers from poor decay of high frequency modes, since the decay tends to 1 as $\alpha \rightarrow -\infty$. Using MCNAB $(\gamma, c) = (\frac{1}{2}, \frac{1}{8})$ the decay tends to $\frac{1}{3}$, which is a significant improvement. See Fig. 4 for these contours.

The contours for SBDF are displayed in Fig. 5. This method has the mildest time-stepping restriction when ν is large and h is small. The decay of high frequency modes is strong, tending to 0 as α tends to $-\infty$. This method, however, has the strictest time step limitation for small $|\alpha|$.

We can now develop a quantitative method for describing time step restrictions for second-order schemes. Such a method will help select which second-order scheme to use for a particular problem.

Defining the mesh Reynolds number [20]

$$(22) \quad R \equiv \frac{ah}{\nu},$$

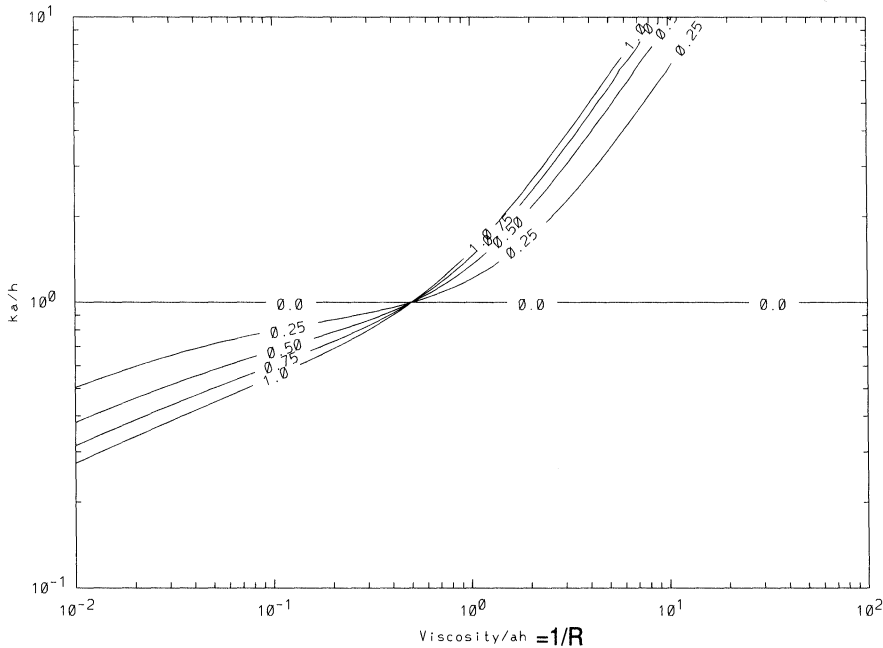


FIG. 6. Time step restriction for various γ where $c = 1 - \gamma$.

in Figs. 6–8 we plot the theoretical time step restrictions for various γ and c . As can be seen from these figures, increasing γ allows larger stable time steps when $R < 2$. The case $c = 1 - \gamma$ also has the property that decreasing γ allows larger time steps for $R > 2$. Comparison of Figs. 6–8 indicates that the largest time step can be applied using SBDF for $R < 2$ and CNLF for $R > 2$. This result physically corresponds to selecting SBDF when discrete diffusion dominates, and CNLF when discrete convection dominates. From this perspective, the popular CNAB is only competitive when $R \approx 2$.

Frequently, an important consideration when choosing a second-order scheme is what the constant of the truncation error is. For example, Crank–Nicolson is known to have a much smaller truncation error than second-order BDF (see, e.g., [12]), so we expect CNAB to have a smaller truncation error than SBDF. The scheme MCNAB is expected to have a truncation error similar to CNAB, however. (Numerical experiments in §4 support this claim.) Because of its small truncation error and because it produces stronger high frequency spatial decay than CNAB, MCNAB may be preferred in certain problems over both CNAB and SBDF when $R < 2$.

One disadvantage that all second-order IMEX schemes with $\gamma > 0$ (i.e., essentially all except CNLF) share is that their stability regions do not contain a portion of the β -axis other than the origin. Specifically, it was shown in [25] that when $\alpha = 0$ one of the roots τ_i of (18) satisfies

$$|\tau_i(\beta k)|^2 = 1 + \left(\gamma^2 + \frac{\gamma}{2} \right) (\beta k)^4 + \dots > 1$$

for βk sufficiently small and $\gamma > 0$. Thus for all k , all second-order schemes such that $\gamma > 0$ are unstable on the nonzero β -axis. The CNLF scheme is well known to be stable on the β -axis provided $k < \frac{h}{a}$, but it is only marginally stable (see, e.g.,

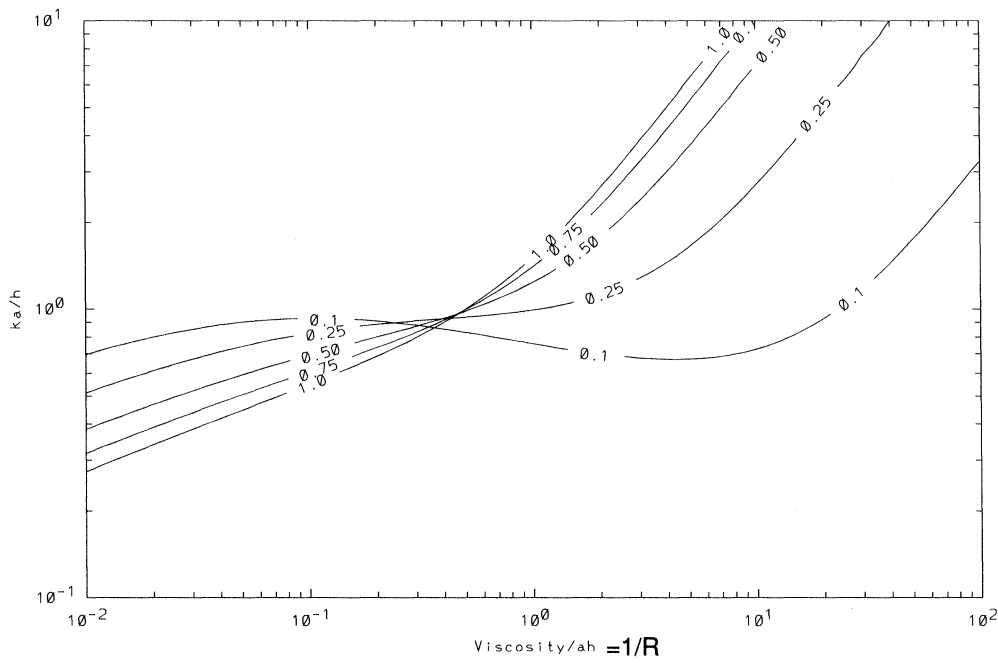


FIG. 7. Time step restriction for various γ where $c = \frac{(1-\gamma)^2}{2}$.

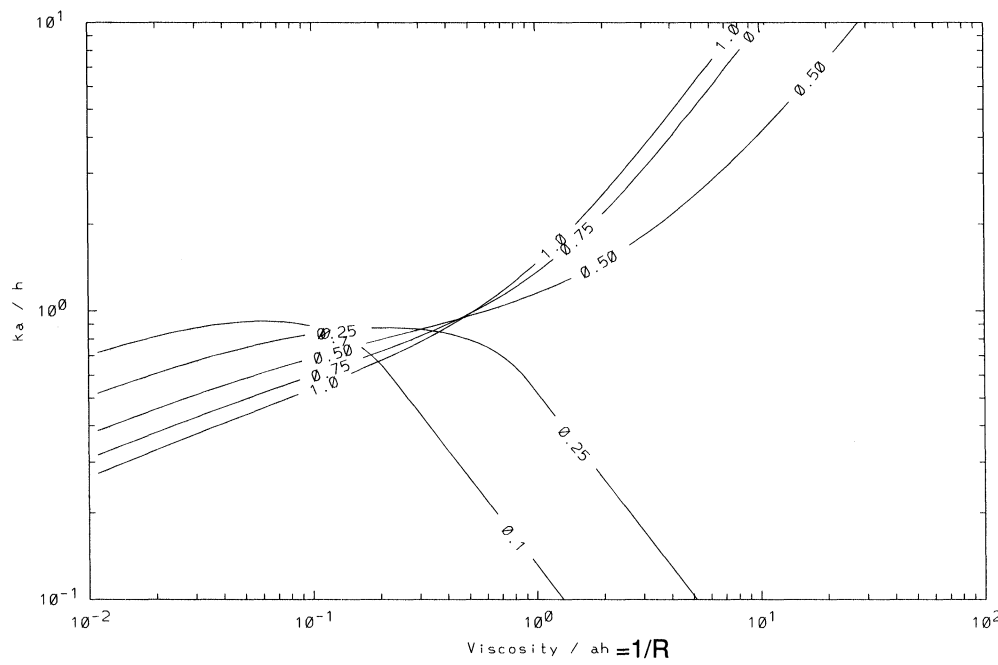


FIG. 8. Time step restriction for various γ where $c = 0$.

[23]), providing no damping of high frequency error components anywhere. To obtain IMEX schemes which are stable for $\nu \geq 0$ and have strong decay for $|\alpha| \gg \frac{1}{k}$ we must consider higher-order schemes.

3.3. Third-order IMEX schemes. Recall from §2 that we have a three-parameter family of three-step IMEX schemes of order three. One possible parameterization yields

$$\begin{aligned}
 (23) \quad & \frac{1}{k} \left[\left(\frac{1}{2}\gamma^2 + \gamma + \frac{1}{3} + \theta \right) u^{n+1} + \left(\frac{3}{2}\gamma^2 - 2\gamma + \frac{1}{2} - \theta \right) u^n \right. \\
 & \quad \left. + \left(\frac{3}{2}\gamma^2 + \gamma - 1 \right) u^{n-1} + \left(-\frac{1}{2}\gamma^2 + \frac{1}{6} \right) u^{n-2} \right] \\
 & = \left(\frac{\gamma^2 + 3\gamma}{2} + 1 + \frac{23}{12}\theta \right) f(u^n) - \left(\gamma^2 + 2\gamma + \frac{4}{3}\theta \right) f(u^{n-1}) \\
 & \quad + \left(\frac{\gamma^2 + \gamma}{2} + \frac{5}{12}\theta \right) f(u^{n-2}) \\
 & \quad + \nu \left[\left(\frac{\gamma^2 + \gamma}{2} + c \right) g(u^{n+1}) + \left(1 - \gamma^2 - 3c + \frac{23}{12}\theta \right) g(u^n) \right. \\
 & \quad \left. + \left(\frac{\gamma^2 - \gamma}{2} + 3c - \frac{4}{3}\theta \right) g(u^{n-1}) + \left(\frac{5}{12}\theta - c \right) g(u^{n-2}) \right].
 \end{aligned}$$

These schemes are centered about time step $(n + \gamma)$ to third order, provided $\theta = 0$. As for lower-order schemes, the value of γ should be between 0 and 1 to avoid large truncation error. Also, the parameter c is multiplied by ν , so this parameter should be adjusted to modify large ν properties of a scheme.

Setting $(\gamma, \theta, c) = (1, 0, 0)$ yields

$$(24) \quad \frac{1}{k} \left(\frac{11}{6}u^{n+1} - 3u^n + \frac{3}{2}u^{n-1} - \frac{1}{3}u^{n-2} \right) = 3f(u^n) - 3f(u^{n-1}) + f(u^{n-2}) + \nu g(u^{n+1})$$

which is the third-order BDF for the implicit part, and therefore is called third-order SBDF.

The third-degree characteristic polynomial resulting from (23) applied to the test equation $\dot{x} = (\alpha + i\beta)x$ is given by

$$\begin{aligned}
 (25) \quad \Phi(z) = & \left[\frac{1}{2}\gamma^2 + \gamma + \frac{1}{3} + \theta - \left(\frac{\gamma^2 + \gamma}{2} + c \right) \alpha k \right] z^3 \\
 & - \left[\frac{3}{2}\gamma^2 + 2\gamma - \frac{1}{2} + \theta + \left(\frac{\gamma^2 + 3\gamma}{2} + 1 + \frac{23}{12}\theta \right) i\beta k + \left(1 - \gamma^2 - 3c + \frac{23}{12}\theta \right) \alpha k \right] z^2 \\
 & + \left[\frac{3}{2}\gamma^2 + \gamma - 1 + \left(\gamma^2 + 2\gamma + \frac{4}{3}\theta \right) i\beta k + \left(\frac{\gamma - \gamma^2}{2} - 3c + \frac{4}{3}\theta \right) \alpha k \right] z \\
 & - \left[\frac{1}{2}\gamma^2 - \frac{1}{6} + \left(\frac{\gamma^2 + \gamma}{2} + \frac{5}{12}\theta \right) i\beta k + \left(\frac{5}{12}\theta - c \right) \alpha k \right].
 \end{aligned}$$

We now determine which methods produce the strongest asymptotic decay as $\alpha \rightarrow -\infty$. For this case, the roots of the characteristic polynomial (25) are given approxi-

mately by

$$(26) \quad \left(\frac{\gamma^2 + \gamma}{2} + c \right) z^3 + \left(1 - \gamma^2 - 3c + \frac{23}{12}\theta \right) z^2 - \left(\frac{\gamma - \gamma^2}{2} - 3c + \frac{4}{3}\theta \right) z + \frac{5}{12}\theta - c = 0.$$

By determining the solutions, τ_1, τ_2 , and τ_3 , of (26) we may evaluate

$$\mathcal{D}_{\gamma, \theta, c} \equiv \max(|\tau_1|, |\tau_2|, |\tau_3|)$$

to obtain an estimate of the high frequency model decay for large ν . Minimization over (γ, θ, c) determines the method with the strongest asymptotic high frequency decay. Certainly if

$$(27) \quad \mathcal{D}_{\gamma_0, \theta_0, c_0} = 0$$

then $(\gamma_0, \theta_0, c_0)$ minimizes the amplification as $\alpha \rightarrow -\infty$. From (26) we satisfy (27) iff

$$(28) \quad \begin{aligned} \frac{1 - \gamma_0^2 - 3c_0 + \frac{23}{12}\theta_0}{\frac{\gamma_0^2 + \gamma_0}{2} + c_0} &= 0, \\ \frac{\frac{\gamma_0^2 - \gamma_0}{2} + 3c_0 - \frac{4}{3}\theta_0}{\frac{\gamma_0^2 + \gamma_0}{2} + c_0} &= 0, \\ \frac{\frac{5}{12}\theta_0 - c_0}{\frac{\gamma_0^2 + \gamma_0}{2} + c_0} &= 0. \end{aligned}$$

Each term is divided by $(\frac{\gamma_0^2 + \gamma_0}{2} + c_0)$ to allow the possibility of satisfying (27) by letting $(\frac{\gamma_0^2 + \gamma_0}{2} + c_0) \rightarrow \pm\infty$. Simplification of the system (28) yields

$$(29) \quad \frac{(3\gamma_0 - 1)(\gamma_0 - 1)}{\frac{\gamma_0^2 + \gamma_0}{2} + c_0} = 0,$$

$$(30) \quad \frac{\theta_0 - 6(\gamma_0^2 - \gamma_0)}{\frac{\gamma_0^2 + \gamma_0}{2} + c_0} = 0,$$

$$(31) \quad \frac{\frac{5}{12}\theta_0 - c_0}{\frac{\gamma_0^2 + \gamma_0}{2} + c_0} = 0.$$

For $(\frac{\gamma_0^2 + \gamma_0}{2} + c_0)$ to be finite there are two possibilities, $(\gamma_0, \theta_0, c_0) = (1, 0, 0)$ and $(\gamma_0, \theta_0, c_0) = (\frac{1}{3}, -\frac{4}{3}, -\frac{5}{9})$, both of which specify third-order SBDF. For $(\frac{\gamma_0^2 + \gamma_0}{2} + c_0)$ to be infinite, (29) implies $|\gamma_0| \ll |c_0|$. Using this in (30) implies $|\theta_0| \ll |c_0|$. Applying these results to (31) results in a contradiction, so $(\frac{\gamma_0^2 + \gamma_0}{2} + c_0)$ must be finite.

Because third-order SBDF has the strongest asymptotic decay of third-order IMEX schemes, special attention is given to its properties throughout the remainder of this section. All schemes considered here are stable on a segment of the β -axis including the origin $(\alpha, \beta) = (0, 0)$, as can be verified by an analysis of (25) [22].

Further information about stability in the α - β plane can be obtained by plotting $\max\{|z| : \Phi(z) = 0\}$, where $\Phi(z)$ is defined in (25). These stability contours are displayed in Figs. 9–14.

We begin by examining if it is possible to arrive at a stable scheme for any fixed γ . For a fixed, but arbitrary, γ and for $|\theta|, |c| \rightarrow \infty$ we obtain an approximate local minimum of $\mathcal{D}_{\gamma, \theta, c}$ if $\frac{c}{\theta} = 0.4661$. Using these parameters, the scheme simplifies to

$$(32) \quad \frac{1}{k}(u^{n+1} - u^n) = \frac{23}{12}f(u^n) - \frac{4}{3}f(u^{n-1}) + \frac{5}{12}f(u^{n-2}) + .4661\nu g(u^{n+1}) \\ + .5184\nu g(u^n) + .0650\nu g(u^{n-1}) - .0494\nu g(u^{n-2})$$

which applies third-order Adams–Bashforth to the explicit term. (Note that γ disappears in (32) through the limiting process.) The stability contours of Fig. 9 suggest that this method is stable for all $\nu \geq 0$ provided $k < 0.62\frac{h}{a}$. This restriction is more severe than that for third-order Adams–Bashforth applied to $\dot{x} = i\beta x$ because of the dip in the stability contours when $\alpha < 0$. As mentioned previously, the β -axis is included in the absolute stability region. This result demonstrates that for third-order methods, it is possible to find methods for any γ which are stable for all $\nu \geq 0$ by varying θ and c .

In §3.2, the most interesting second-order schemes were produced by selecting γ equal to 0, $\frac{1}{2}$, or 1. We consider schemes for these values of γ below. The parameters θ and c are chosen to produce schemes which allow large stable time steps as $\nu \rightarrow \infty$.

For example, the method $(\gamma, \theta, c) = (0, -2.036, -.876)$ of Fig. 10 is stable for all $\nu \geq 0$ provided $k \leq 0.67\frac{h}{a}$. Similarly $(\gamma, \theta, c) = (.5, -1.21, -.5)$ of Fig. 12 is stable for all $\nu \geq 0$ if $k \leq 0.65\frac{h}{a}$. In both these cases substantially larger time steps can be taken for large or moderate $|\alpha|$ than for the method (32). Furthermore, stronger high frequency decay occurs for these methods than for method (32).

Recall that the strongest decay as $\alpha \rightarrow -\infty$ occurs for third-order SBDF. The stability contours for this method are shown in Fig. 13. This plot together with the zoom-in of Fig. 14 suggest that third-order SBDF is stable for all $\alpha \leq 0$ provided $k < 0.62\frac{h}{a}$. The plot of Fig. 13 also indicates that very large time steps can be taken for large or moderate $|\alpha|$. Although applying $\gamma = 1$ and nonzero θ and c may allow somewhat larger stable time steps we focus on $\theta = c = 0$ since other choices degrade the strong asymptotic decay.

For $\gamma \neq 1$, the choice $\theta = c = 0$ is not recommended. As seen in Fig. 11, $(\gamma, \theta, c) = (\frac{1}{2}, 0, 0)$ results in a small stability region. This plot indicates that very small time steps are needed for moderate or large $\frac{\nu}{h^2}$, since the ellipse of Fig. 1 must lie in the stable region.

3.4. Fourth-order IMEX schemes and a comparison. From §2, the general fourth-order, four-step IMEX scheme is a four parameter family of methods. From the previous section we anticipate that the fourth-order SBDF may have good stability properties. For $\dot{u} = f(u) + \nu g(u)$, this scheme is given by

$$(33) \quad \frac{1}{k} \left(\frac{25}{12}u^{n+1} - 4u^n + 3u^{n-1} - \frac{4}{3}u^{n-2} + \frac{1}{4}u^{n-3} \right) \\ = 4f(u^n) - 6f(u^{n-1}) + 4f(u^{n-2}) - f(u^{n-3}) + \nu g(u^{n+1}).$$

The characteristic polynomial obtained from applying (33) to $\dot{x} = (\alpha + i\beta)x$ is

$$\Phi(z) = \left(\frac{25}{12} - \alpha k \right) z^4 - (4 + 4i\beta k) z^3 + (3 + 6i\beta k) z^2 - \left(\frac{4}{3} + 4i\beta k \right) z + \frac{1}{4} + i\beta k.$$

Contour plots similar to those in Figs. 13 and 14 were obtained for the fourth-order SBDF as well (see [22] for these plots). The scheme is stable for $k \leq 0.52\frac{h}{a}$ and

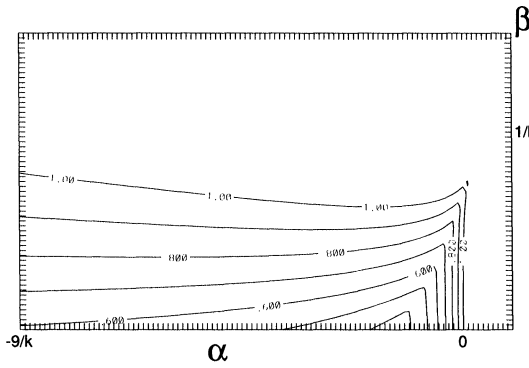


FIG. 9. Stability contours for $(\gamma, \theta, c) = \lim_{\theta \rightarrow \infty} (\gamma, \theta, .4661\theta)$.

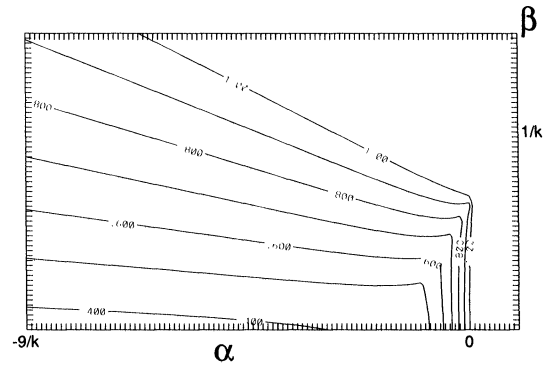


FIG. 10. Stability contours for $(\gamma, \theta, c) = (0, -2.036, -.876)$.

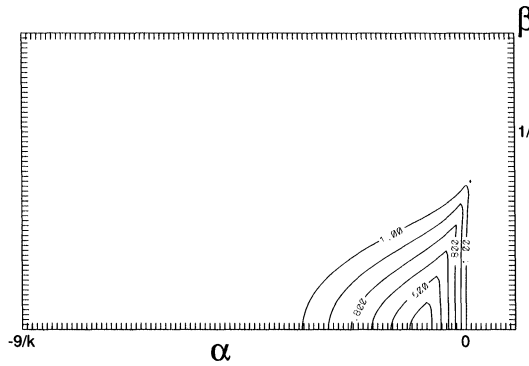


FIG. 11. Stability contours for $(\gamma, \theta, c) = (\frac{1}{2}, 0, 0)$.

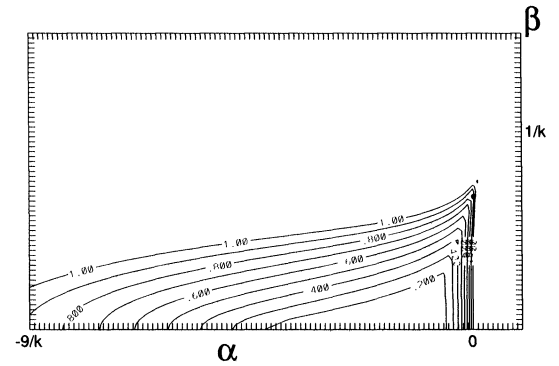


FIG. 12. Stability contours for $(\gamma, \theta, c) = (\frac{1}{2}, -1.21, .5)$.

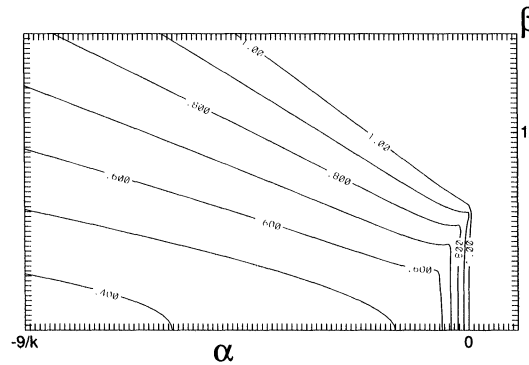


FIG. 13. Stability contours for 3rd order SBDF, $(\gamma, \theta, c) = (1, 0, 0)$.

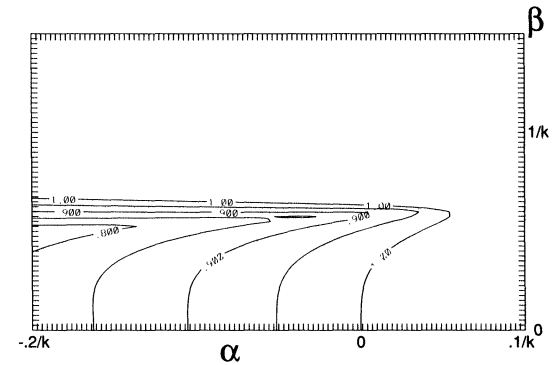


FIG. 14. Zoom-in around $\alpha = 0$ for 3rd Order SBDF.

larger time steps are permitted as ν increases. However, the stability region is smaller than for the third-order case, so smaller time steps may be required. Furthermore, the β -axis is closer to the boundary of the stability region for fourth-order SBDF, suggesting that third-order SBDF may dissipate error better for $\nu \approx 0$.

Third- and fourth-order SBDF methods are good choices for IMEX schemes for some problems. For all $\nu \geq 0$, these methods are stable for a time step restriction

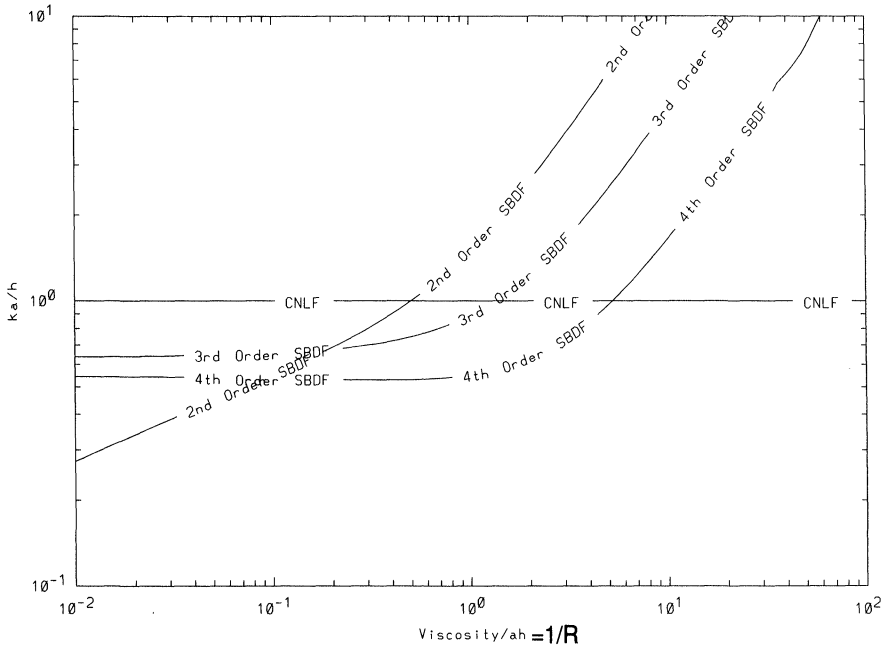


FIG. 15. Time step restrictions for various IMEX schemes.

similar to the CFL condition. Greater accuracy and strong high frequency decay also make these methods very attractive. Nonetheless, for many problems second-order methods are preferred. Higher-order methods require more storage, and more work per time step. This extra expense could be justified if greater accuracy permitted larger time steps. Third- and fourth-order schemes, however, have more severe time step restrictions than second-order schemes. In fact, Fig. 15 shows that larger stable time steps can be taken with second-order SBDF when $R < 9$ for the linear advection-diffusion problem using second-order spatial discretizations. CNLF allows larger stable time steps than either third- or fourth-order SBDF for $R > 1$.

Third-order SBDF should be efficient for problems which require strong decay for $|\alpha| \gg \frac{1}{k}$ and a moderate time step restriction for $R > 10$. It should also be effective for problems where $R \gg 1$, since a portion of the β -axis is within the stability region.

Fourth-order SBDF has a particularly severe time step restriction for the advection-diffusion problem when R is moderate or small. For example, when $R = .125$, fourth-order SBDF can only apply one tenth the time step of second-order SBDF, as can be seen from Fig. 15. This restriction on the step size would appear to limit fourth-order SBDF to problems where accuracy, and not stability, is the reason for limiting the time step size.

4. Further considerations and numerical experiments. The previous section has dealt with stability properties of IMEX schemes for the one-dimensional linear constant coefficient advection-diffusion equation. These results provide necessary, but not sufficient conditions for stability for variable coefficient and nonlinear convection-diffusion problems.

In this section we summarize numerical experiments which verify that our analysis for the simple, linear problem can be useful for determining which IMEX scheme to

apply to more complicated problems. In addition, strongly damping schemes are shown to be more efficient in certain spectral collocation and multigrid applications. In order to calculate starting values for multistep IMEX schemes, we use one-step (low-order) IMEX schemes with a very small time step, unless otherwise noted.

4.1. Finite difference approximations in one dimension.

Example 1. To examine nonzero viscosity behaviour, we consider the one-dimensional variable coefficient problem

$$(34) \quad u_t + \sin(2\pi x)u_x = \nu u_{xx}$$

subject to periodic boundary conditions on the interval $[0,1]$ and initial condition

$$u(x, 0) = \sin(2\pi x).$$

We use centered second-order differences for the spatial derivatives. Note that the solution is smooth for all $\nu \geq 0$.

To test the theory's predictions for small mesh Reynolds numbers (22), the model problem (34) was approximately solved using discretization step sizes $h = \frac{1}{63}$ in space and $k = 1.8h$ in time. Use of such step sizes is appropriate only for strongly damped flow. Utilizing several IMEX schemes, computations to time $t = 2$ are performed for viscosities ν in the range $.01 \leq \nu \leq .1$. These values correspond to mesh Reynolds numbers R in the range $1.59 \geq R \geq 0.159$.

From Figs. 6, 7, 8, and 15 the theory predicts that for these step sizes SBDF is stable for a larger viscosity interval than any other scheme. As ν decreases, third-order SBDF followed by CNAB should become unstable. Stability for MCNAB should be similar to, and somewhat better than, CNAB. Furthermore, fourth-order SBDF and CNLF should be unstable over the entire interval because the theoretical stability restriction is violated.

By comparing results with those for $h = \frac{1}{504}$ and $k = .225h$ using SBDF, the max norm relative errors for second-order schemes are evaluated. Third- and fourth-order schemes are compared with computations with these same step sizes but using third- and fourth-order SBDF. The resultant errors are plotted against ν in Fig. 16. Fourth-order SBDF and CNLF are not included because they are unstable over the entire interval. The plots of the figure clearly coincide with the results of the theory.

Figure 16 also indicates that SBDF is the only stable method for the above choice of discretization parameters when $0.0015 < \nu < 0.0025$. (The values of ν where the curves turn upward correspond to the onset of instability for the given values of h and k .) This agrees with the prediction that SBDF allows the largest stable time steps for small mesh Reynolds numbers (see §3.2). Although third-order SBDF has a smaller stability interval, it may be useful in problems where high accuracy is needed since it produces a smaller error than second-order methods when stable.

To test the theory's predictions for large mesh Reynolds numbers, example (34) was solved using discretization step sizes $h = \frac{1}{81}$ in space and $k = .9h$ in time. Using several IMEX schemes, computations to time $t = 2$ are performed for viscosities ν in the range $.001 \leq \nu \leq .01$. These values correspond to mesh Reynolds numbers R in the range $12.3 \geq R \geq 1.23$.

From Figs. 6, 7, 8, and 15 the theory predicts that for these step sizes only CNLF is stable over the entire viscosity interval. As ν decreases, third-order SBDF followed by SBDF and finally CNAB should become unstable. Stability for MCNAB should be similar to CNAB. Furthermore, fourth-order SBDF should be unstable over the

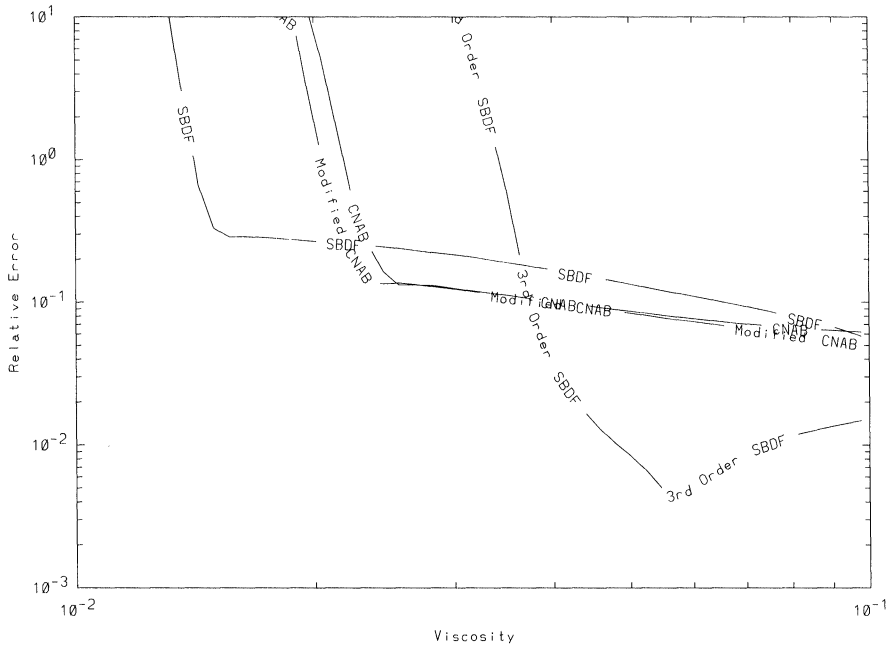


FIG. 16. Large viscosity behaviour for various IMEX methods.

entire interval because the theoretical stability restriction is violated when $\nu < .05$ for these step sizes.

By comparing results with those for $h = \frac{1}{648}$ and $k = .225h$ using SBDF, the max norm relative errors for second-order schemes are evaluated for these computations. Third- and fourth-order schemes are compared with computations with these same step sizes but using third- and fourth-order SBDF. The resultant errors are plotted against ν in Fig. 17. Fourth-order SBDF is not plotted because it is unstable over the entire interval. The plots of the figure support the results of the theory.

Figure 17 also indicates that CNLF is the only stable method for $\nu < 0.002$. This agrees with the prediction that CNLF allows the largest stable time steps for large mesh Reynolds numbers (see §3.2). CNLF is a particularly attractive choice because it has the smallest error of second-order methods. Use of SBDF is not recommended because it has the smallest stable interval and the largest error among any of the second-order schemes considered.

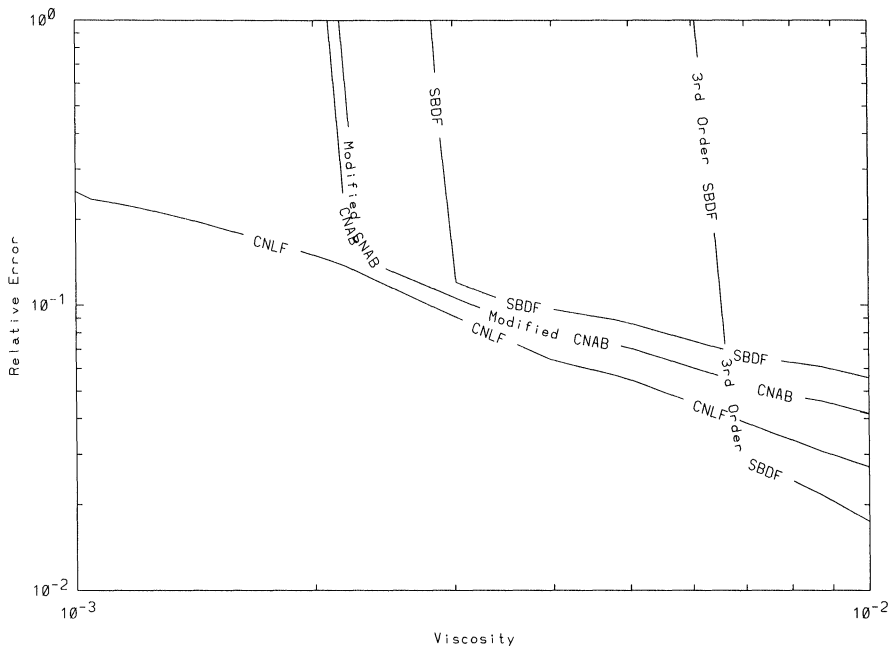
For the same problem using $k = .5h$, dramatically different results are predicted because all the methods satisfy their theoretical stability restrictions. Indeed, computations for CNLF, third- and fourth-order SBDF all produce errors which nearly coincide, since spatial error dominates the solutions. Other second-order methods appear stable and produce only slightly less accurate results. \square

Example 2. To examine the limit $\nu = 0$, we consider the one-dimensional nonlinear problem

$$(35) \quad u_t + \frac{1}{2} \cos(2\pi t)(1 + u)u_x = 0$$

having periodic boundary conditions on the interval $[0,1]$ and initial conditions

$$u(x, 0) = \sin(2\pi x).$$

FIG. 17. *Small viscosity example for various IMEX methods.*

As in the previous two sections, we use second-order centered differences to approximate u_x . For $h = \frac{1}{80}$ and $k = .5h$, computations are performed to time $t = 100$. The time step value $k = .5h$ was used to ensure that fourth-order SBDF satisfied the stability restriction $k \leq .52h$. Using the fact that the exact solution to this problem at integer t equals the initial data, i.e.,

$$u(x, n) = \sin(2\pi x), \quad n = 0, 1, 2, \dots,$$

we compute the error in the solution at time $t = n, n = 1, 2, \dots, 100$.

The results again agreed with the predictions from §3: All second-order schemes tested, such that $\gamma > 0$, were unstable, while CNLF, third-order SBDF, and fourth-order SBDF were all stable. The SBDF schemes are dissipative as well. For fuller details, see [22]. \square

4.2. Spectral collocation.

Example 3. For our next application we consider the well-known Burgers equation

$$(36) \quad u_t + uu_x = \nu u_{xx}$$

subject to periodic boundary conditions on the interval $[-1, 1]$ and initial conditions

$$u(x, 0) = \sin(\pi x).$$

A plot of the solution of the Burgers equation for $\nu = .01$ at several different times is provided in Fig. 18. This computation was produced using Chebyshev collocation with 40 basis functions and $k = 1/160$ using SBDF.

The next few subsections discuss Fourier and Chebyshev collocation implementations for the above model problem. See [7] or [3] for details on these methods.

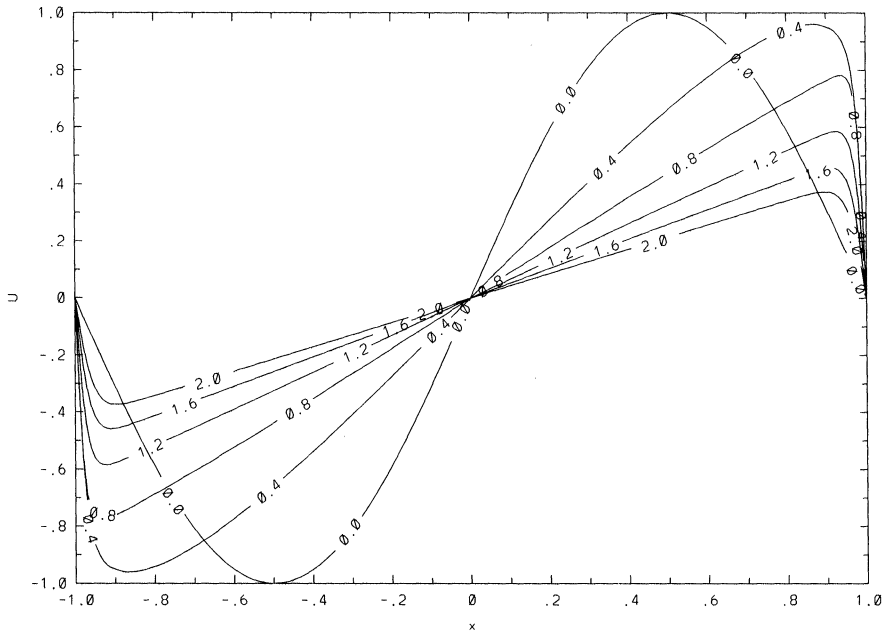


FIG. 18. Burgers equation for various t for $\nu = 0.01$.

4.2.1. Fourier spectral collocation. Since the problem of Example 3 is periodic, we expect that Fourier series makes a good basis of trial functions for this problem. Indeed, since

$$u_t = -\frac{1}{2} \frac{\partial u^2}{\partial x} + \nu \frac{\partial^2 u}{\partial x^2}$$

we see that u_t is antisymmetric for u antisymmetric. By selecting an initial condition which is antisymmetric we guarantee that u remains antisymmetric for all t . Since only these components of the series contribute to the solution we use a Fourier sine series. We thus approximate u by the series

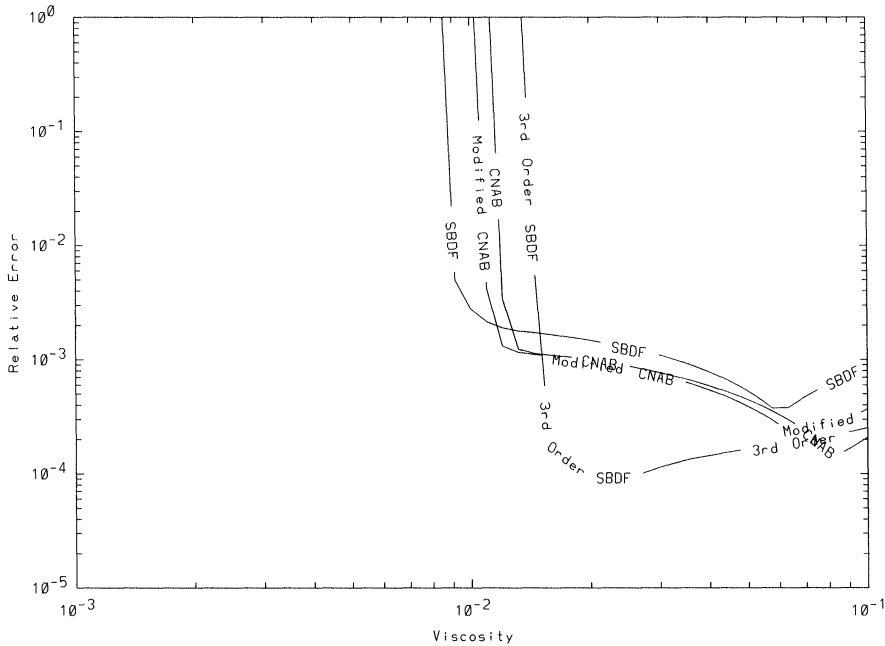
$$u_N(x, t) = \sum_{j=1}^N \alpha_j(t) \sin(jx).$$

Using initial conditions $\alpha_1(0) = 1$, $\alpha_k(0) = 0$, and $k \neq 1$, the $\alpha_j(t)$ are determined by enforcing the differential equation at the collocation points $x_j = \frac{j}{N} - \frac{1}{2N}$, $1 \leq j \leq N$, i.e.,

$$\left[\frac{\partial u_N}{\partial t} + u_N \frac{\partial u_N}{\partial x} = \nu \frac{\partial^2 u_N}{\partial x^2} \right]_{x=x_j}.$$

This scheme is also called a pseudospectral method since the nonlinear convection term is evaluated in physical space.

By applying Fourier sine collocation with 40 basis functions and $k = 1/40$, we solve the model problem at each time step to time $t = 2$. Because the system is small, the implicit equations are solved in physical space using LU decomposition. In larger

FIG. 19. *Fourier spectral collocation for Burgers equation.*

systems where greater efficiency is needed these would be solved in Fourier space using transform methods (see [7]). For CNAB, MCNAB, SBDF, and third-order SBDF the max norm relative error is plotted against viscosity (see Fig. 19). The “exact solution” is based on a computation using $N = 80$ modes and $k = \frac{1}{3200}$ and third-order SBDF.

CNLF was not included because the theoretical stability restriction is violated. This can be easily seen because the linear advection-diffusion equation has eigenvalues $(ian\pi - \nu n^2\pi^2)$ for eigenfunctions $e^{in\pi x}$. From these eigenvalues we know that the stability restriction is $k < \frac{1}{an\pi}$, which is violated initially because $|u(x, 0)|_\infty = 1$.

As expected, third-order SBDF has the smallest error of any of the methods when stable. The stable region, however, is smaller than that for CNAB or SBDF. CNAB and MCNAB are once again very similar in behavior with the modified version being marginally better. SBDF appears to allow the largest stable time step when $\nu \approx 0.01$.

Further refinement of the time step to $k = \frac{1}{160}$ leaves third-order SBDF as the method of choice over the entire interval. Such a refinement may be unnecessary in this example because the error is less than 1% for a step size which is four times larger.

4.2.2. Chebyshev spectral collocation. Because the solution to the problem is periodic and antisymmetric we know that $u(\pm 1, t) = 0$ for all t . Using this fact, we solve (36) subject to the homogeneous Dirichlet boundary conditions $u(\pm 1, t) = 0$, using a pseudospectral Chebyshev collocation scheme. The Gauss–Chebyshev grid

$$x_i = \cos[(2i - 1)\pi/2N], \quad i = 1, \dots, N$$

is used for collocation points.

Similar to the Fourier case, the max norm relative errors are evaluated for several IMEX schemes using $k = 1/40$ and $N = 40$. As can be seen from Fig. 20, the results

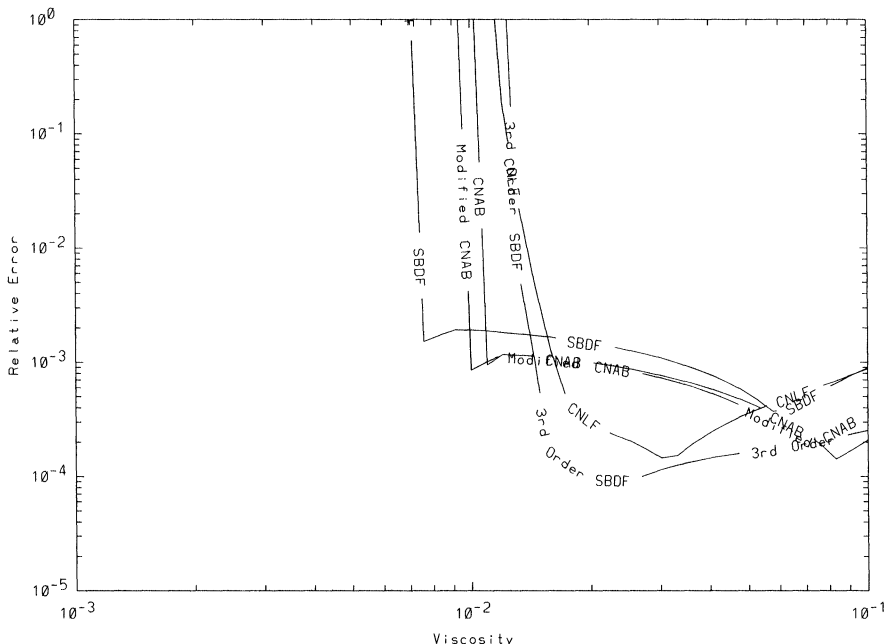


FIG. 20. Chebyshev spectral collocation for Burgers equation.

are qualitatively similar to those of the Fourier case. SBDF performs particularly well for smaller viscosities. From the theory, it has the widest stability region for large $|\alpha|$ and thus is best able to accommodate the rapidly growing eigenvalues associated with Chebyshev collocation.

Both Chebyshev and Fourier collocation can be affected by aliasing [7]. We consider aliasing for the Fourier case next.

4.2.3. Aliasing in pseudospectral methods. Aliasing occurs when nonlinear terms produce frequencies that cannot be represented in the basis, and thus contribute erroneously to lower frequencies. For instance, in Example 3, the Fourier sine mode $\sin(mx)$ when explicitly evaluated in the convection term produces the contribution

$$\sin(mx) \frac{\partial \sin(mx)}{\partial x} = \frac{m}{2} \sin(2mx).$$

If $2m$ is greater than the number of Fourier sine basis functions N , this frequency cannot be represented correctly and aliasing occurs. We now proceed to demonstrate that this behavior can plague poorly spatially resolved computations when applying weakly damping IMEX schemes.

We compute solutions for the model Burgers equation (36) subject to periodic boundary conditions and the initial conditions of Example 3 modified to read

$$u(x, 0) = 0.98 \sin(2\pi x) + HF(x)$$

where

$$HF(x) \equiv 0.01 \sin(61\pi x) + 0.01 \sin(62\pi x).$$

We use Fourier sine collocation with $N = 64$ basis functions, and integrate to time $t = 2$ with a viscosity $\nu = 0.1$.

TABLE 1

k	CNLF	CNAB	MCNAB	SBDF	3 rd order SBDF
$\frac{1}{64}$.92	.575	.0056	.0072	.0045
$\frac{1}{192}$.060	.022	.0013	.00079	.0010

The value of the approximate solution at time $t = k$ is obtained using first-order SBDF with the same step size. To represent the type of high frequency information that could be produced during a computation, we add $HF(x)$ to the solution at $t = k$. This ensures that high frequency information remains after the strongly damping first-order SBDF step. Subsequent steps are then computed using the relevant second-order scheme. For third-order SBDF, the value at $t = 2k$ is also needed. For the purpose of demonstrating aliasing effects, this value is computed using CNAB since we wish to retain most of the added high frequencies.

The max norm relative errors for several IMEX schemes are computed by comparing results with those for SBDF using $N = 128$ and $k = \frac{1}{24N}$. In the third-order case, results are compared with those for third-order SBDF using $N = 128$ and $k = \frac{1}{24N}$. These errors are summarized in Table 1.

For the case $k = \frac{1}{64}$ we note that the error for CNAB is far greater than for MCNAB, SBDF, or third-order SBDF. Using CNAB, a nonaliased computation using the 2/3's rule [7] and $k = \frac{1}{64}$ results in a relative error of less than 10^{-3} . This nonaliased result, along with its aliased counterpart, are plotted in Fig. 21. The "error" curve in this figure is that of the aliased CNAB. From the figure it is clear that the main component of the error is proportional to $\sin(\pi x)$. This low frequency mode is not part of the exact solution and must be an aliasing artifact from high frequency components. It is interesting to note that even after 128 time steps the numerical solution is still plagued by high frequency components which have not yet decayed. A similar study of CNLF reveals that it suffers from aliasing as well.

Resorting to a smaller time step $k = \frac{1}{192}$ makes a substantial improvement in the solution for CNAB and CNLF. Even so, the aliasing error for CNLF is sufficiently large that further refinement is likely required.

We conclude that use of a strongly damping scheme such as SBDF, MCNAB, or third-order SBDF gives an inexpensive method to reduce aliasing in poorly resolved computations. Application of weakly damping schemes like CNAB and especially CNLF may necessitate undesirably small time steps to produce the high frequency decay needed to prevent aliasing in an aliased computation. Alternatively, weakly damping schemes may be used in conjunction with an antialiasing technique such as the 3/2's rule or the 2/3's rule [7]. However, these antialiasing techniques either increase the expense of the computation or produce a severe loss of high frequency information at each time step. \square

Remark. It may be argued that our addition of the high frequency components to the numerical solution is artificial. However, this allows us to study the propagation of errors related to these effects in simple examples within a controlled environment. In general, high frequency solution and error components are generated at each time step by nonlinear terms, forcing terms, and boundary effects (cf. [6]). \square

4.3. Time-dependent multigrid in two spatial dimensions.

Example 4. The next model that we consider is the two-dimensional convection-diffusion problem

$$(37) \quad \mathbf{u}_t + (\mathbf{u} \cdot \nabla) \mathbf{u} = \nu \Delta \mathbf{u}$$

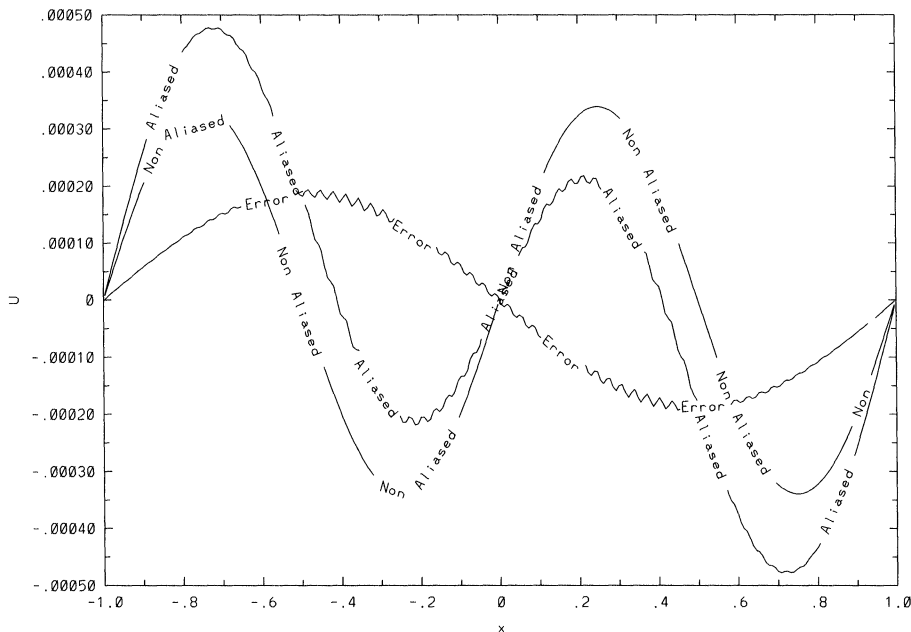


FIG. 21. Aliased and non-aliased computations for CNAB.

where $\mathbf{u} \equiv (u, v)$. This model incorporates some of the major ingredients of the two-dimensional Navier–Stokes equations. Indeed, it is often being solved as part of projection schemes for incompressible flows (see [13]). We carry out our computations on the square $\Omega \equiv [0, 1] \times [0, 1]$ and consider periodic boundary conditions and the initial conditions

$$u(x, y, 0) = \sin[2\pi(x + y)],$$

$$v(x, y, 0) = \sin[2\pi(x + y)].$$

For spatial discretization we use standard second-order centered differences as before. For IMEX schemes the convection term, $(\mathbf{u} \cdot \nabla)\mathbf{u}$ is handled explicitly and the diffusion term $\nu \Delta \mathbf{u}$ is handled implicitly. This treatment yields a positive definite, symmetric, sparse linear system to solve at each time step. Such systems are solved efficiently using a multigrid algorithm, the components of which are outlined next.

To solve the implicit equations we apply a full multigrid (FMG), full approximation scheme (FAS) algorithm [5]. Rather than applying the standard algorithm at each time step, we use the ideas of [6]. Smoothing is accomplished using red-black Gauss–Seidel. This relaxation technique is chosen because it has a very good smoothing rate. Prolongation is accomplished using bilinear interpolation and restriction by full weighting. The standard FMG cycle is modified so that the first coarse grid correction is performed before any fine grid relaxation. Based on the assumption that the increment between time steps is smooth, fine grid relaxation is most effective after the smoothness of the increment is accounted for (see [6]). Interpolation for the FMG step is bilinear. In [6] it is argued that for time-dependent problems higher-order interpolation only decreases high frequency error, which tends to dissipate in parabolic systems anyway. This suggestion is utilized here; indeed experiments with

cubic interpolation did not produce any reduction in the number of multigrid iterations to achieve a given tolerance. Another recommendation of [6] is to avoid the final smoothing pass at each time step in order to reduce aliasing from red-black Gauss-Seidel relaxation. Aliasing is not a major source of error in Example 4, however, so this suggestion was not utilized.

For this problem we use a residual test with a tolerance TOL to determine the number of fine grid iterations to perform at each time step. Next we show that the choice of time-stepping scheme can affect the number of fine grid iterations to achieve a given residual tolerance.

The model problem (37) was approximated using step sizes $h = \frac{1}{128}$ and $k = 0.00625$ and residual tolerance TOL=0.003. After the first time step, high frequency information

$$HF(x, y) = 0.005 \cos[2\pi(64x + 63y)]$$

was added to each of u and v to represent the type of high frequency information that might be produced during a computation.

For several second-order IMEX schemes, the average number of fine grid iterations at each time step was computed. The result using V-cycles is graphed in Fig. 22. Strongly damping schemes such as SBDF and MCNAB require roughly one iteration per time step. Weakly damping schemes required far more effort to solve the implicit equations accurately, because lingering high frequency components necessitate more work on the finest grid. This is evident since CNAB requires more than two iterations per time step and CNLF required three.

Using a W-cycle improves the relative efficiencies of CNLF and CNAB. Even for these cases, however, nearly twice the number of fine grid iterations were required than for more strongly damping schemes such as SBDF and MCNAB. See [22] for a plot.

Even for a smaller viscosity $\nu = 0.02$ and a much coarser mesh $h = \frac{1}{32}$, the performance of CNLF suffers. It uses about 30% more iterations than SBDF or MCNAB to achieve the desired tolerance. This result uses TOL=.009 and is plotted in Fig. 23.

Thus we conclude that use of a poorly damping IMEX scheme such as CNAB or especially CNLF can necessitate extra iterations on the finest grid in multigrid solutions to the implicit equations for small mesh Reynolds numbers $R < 2$. For large mesh Reynolds numbers $R > 2$, this effect was not observed. \square

5. Conclusions and recommendations. IMEX schemes are not a universal cure for all problems. It is not difficult to imagine situations where a fully implicit or fully explicit scheme is preferable. However, these schemes can be very effective in many situations, some of which are depicted in this paper.

It may be important to choose an IMEX scheme carefully. The usual CNAB can be significantly outperformed by other IMEX schemes. Based on observations in this and previous sections we provide a few guidelines for selecting IMEX schemes for convection-diffusion problems.

5.1. Finite differences. For the finite difference (finite element, finite volume) case, begin by determining an estimate for the mesh Reynolds number $R = \frac{ah}{\nu}$ where ν represents viscosity, a represents characteristic speed, and h represents grid spacing.

For problems where $R \gg 2$ application of CNLF, or a third- or fourth-order scheme is reasonable. Third- and fourth-order SBDF can be applied to these problems,

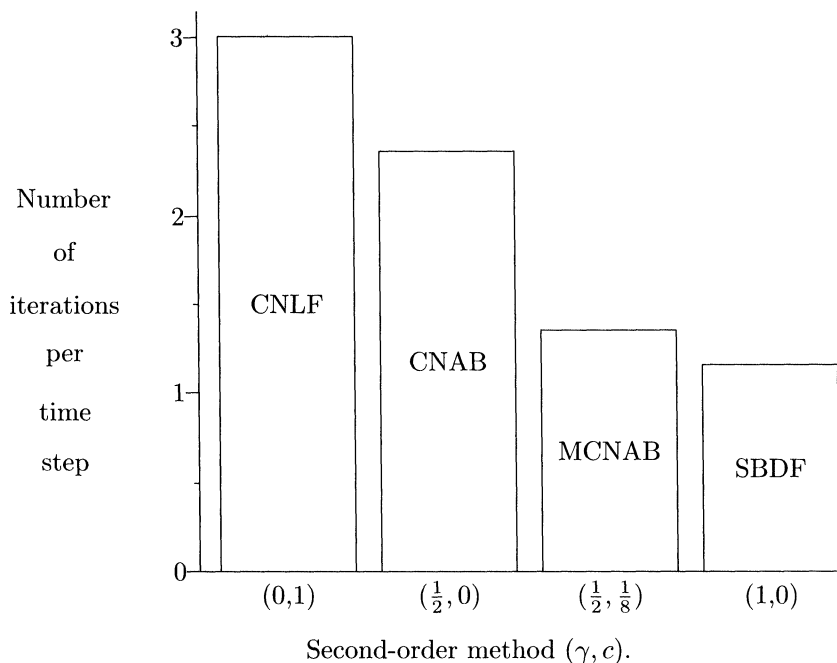


FIG. 22. Multigrid V-cycle iterations, $\nu = 0.03, h = \frac{1}{128}$.

since a portion of the β -axis is included in the stability region even though these methods were selected primarily for their large ν properties. Of the methods we have considered in detail, CNLF has the mildest time step restriction and is nondissipative while third-order SBDF is the most dissipative. All other second-order schemes should be avoided in this case. Explicit schemes should also be considered for these problems.

For $R > 2$ use of CNLF or third-order SBDF appears appropriate. CNLF has the mildest time step restriction, but accuracy concerns could make third-order SBDF competitive. Avoid use of SBDF in this case. For problems of this type, a study to determine when explicit schemes are competitive would be interesting.

For $R \approx 2$ the theory predicts that many second-order IMEX schemes have similar time step restrictions. A study to determine the method with the smallest truncation error would be useful in this case. For greater accuracy, third-order SBDF appears to be more useful than fourth-order SBDF, since its time step restriction is less severe. If strong decay of high frequency spatial modes is a desirable characteristic then CNLF should be avoided.

For $R < 2$, use of SBDF permits the largest stable time steps. The modified CNAB scheme, MCNAB, can also be applied to problems of this type, although its time step restriction is somewhat stricter. third-order SBDF is recommended when high accuracy is needed. Numerical experiments in §4.3 demonstrate that in multigrid solutions to the implicit equations, application of a strongly damping method is prudent. MCNAB or SBDF should be useful in such problems. Avoid use of CNLF in this case.

5.2. Spectral methods. Because the eigenvalues for spectral methods are different than for finite differences as is their meaning (see [24]), we cannot expect the stability time step restrictions from §3 to hold quantitatively. For this reason, an

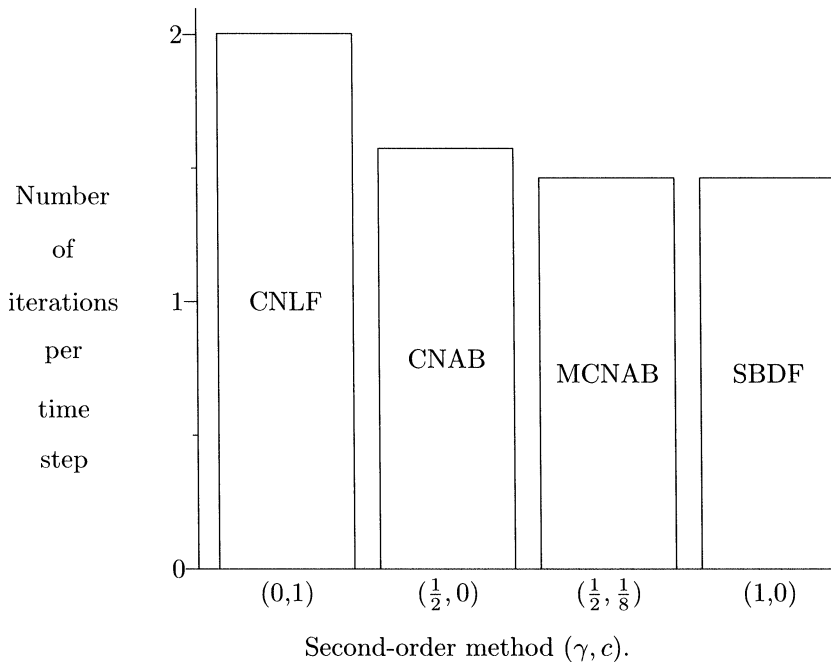


FIG. 23. Multigrid W -cycle iterations, $\nu = 0.02$, $h = \frac{1}{32}$.

analysis of the linear advection-diffusion equation for Chebyshev and Fourier spectral methods would be interesting. However, this is outside the scope of this paper.

Numerical experiments for the Burgers equation were made for small to moderate mesh Reynolds numbers. For these problems, CNLF has a very severe time step restriction. These computations also suggest that SBDF has the mildest time step restriction of the methods considered. This result is particularly pronounced in the Chebyshev collocation case.

The large mesh Reynolds number case for spectral collocation was not considered. In this case, a comparison of the relative efficiencies of IMEX schemes and fully explicit schemes would be interesting.

Third-order SBDF appears to be an efficient method for problems where high accuracy is needed.

In problems where aliasing occurs, a strongly damping scheme, such as SBDF, MCNAB, or third-order SBDF can be used to inexpensively reduce aliasing. Application of a weakly damping scheme such as CNAB or CNLF in poorly spatially resolved aliased computations should be avoided.

REFERENCES

- [1] L. ABIA AND J. SANZ-SERNA, *The spectral accuracy of a fully-discrete scheme for a nonlinear third-order equation*, Computing, 44 (1990), pp. 187–196.
- [2] C. BASDEVANT, M. DEVILLE, P. HALDENWANG, J. LACROIX, J. OUAZZANI, R. PEYRET, P. ORLANDI, AND A. PATERA, *Spectral and finite difference solutions of the Burgers equation*, Comput. Fluids, 14 (1986), pp. 23–41.
- [3] J. BOYD, *Chebyshev & Fourier Spectral Methods*, Springer-Verlag, Berlin, New York, 1989.
- [4] M. BRACHET, D. MEIRON, S. ORSZAG, B. NICKEL, R. M. ORF, AND U. FRISCH, *Small-scale structure of the Taylor-Green vortex*, J. Fluid Mech., 130 (1983), pp. 411–452.

- [5] A. BRANDT, *Guide to multigrid development*, in Multigrid Methods, W. Hackbusch and U. Trottenberg, eds., Springer-Verlag, Berlin, 1982, pp. 220–312.
- [6] A. BRANDT AND J. GREENWALD, *Parabolic multigrid revisited*, in Multigrid Methods III, W. Hackbusch and U. Trottenberg, eds., Birkhäuser-Verlag, Basel, Boston, 1991, pp. 143–154.
- [7] C. CANUTO, M. HUSSAINI, A. QUARTERONI, AND T. ZANG, *Spectral Methods in Fluid Dynamics*, Springer-Verlag, Berlin, New York, 1987.
- [8] M. CROUZEIX, *Une méthode multigras implicite-explicite pour l'approximation des équations d'évolution paraboliques*, Numer. Math., 35 (1980), pp. 257–276.
- [9] C. GEAR, *The automatic integration of stiff ordinary differential equations*, in Proc. IFIP Congress 1968, A. Morrell, ed., North Holland Publishing Company, Amsterdam, 1969, pp. 187–193.
- [10] B. GUSTAFSSON AND P. LOTSTEDT, *Fourier analysis of multigrid methods for general systems of PDEs*, Math. Comp., 60 (1993), pp. 473–493.
- [11] W. HACKBUSCH, *Multi-Grid Methods and Applications*, Springer-Verlag, Berlin, New York, 1985.
- [12] E. HAIRER, S. NORSETT, AND G. WANNER, *Solving Ordinary Differential Equations I*, Springer-Verlag, Berlin, New York, 1987.
- [13] C. HIRSCH, *Numerical Computation of Internal and External Flows*, Wiley, New York, 1988.
- [14] A. JAMESON, *Computational transonics*, Comm. Pure Appl. Math., XLI (1988), pp. 507–549.
- [15] G. KARNIADAKIS, M. ISRAELI, AND S. ORSZAG, *High-order splitting methods for the incompressible Navier-Stokes equations*, J. Comput. Phys., 97 (1991), pp. 414–443.
- [16] J. KIM AND P. MOIN, *Application of a fractional-step method to incompressible Navier-Stokes equations*, J. Comput. Phys., 59 (1985), pp. 308–323.
- [17] H. KREISS, *Numerical methods for solving time-dependent problems for partial differential equations*, Lecture Notes, Univ. de Montreal, 1978.
- [18] P. MEEK AND J. NORBURY, *Two-stage, two-level finite difference schemes for nonlinear parabolic equations*, IMA J. Numer. Anal., 2 (1982), pp. 335–356.
- [19] J. MURRAY, *Mathematical Biology*, Springer-Verlag, Berlin, New York, 1989.
- [20] R. PEYRET AND T. TAYLOR, *Computational Methods for Fluid Flow*, Springer-Verlag, Berlin, New York, 1983.
- [21] S. RUUTH, *Implicit-explicit methods for reaction-diffusion problems*, J. Math. Biol., submitted.
- [22] ———, *Implicit-Explicit Methods for Time-Dependent PDE's*, master's thesis, Ins. Appl. Math., Univ. of British Columbia, Vancouver, 1993.
- [23] J. STRIKWERDA, *Finite Difference Schemes and Partial Differential Equations*, Brooks/Cole, Pacific Grove, CA, 1989.
- [24] L. TREFETHEN, *Lax-stability vs. eigenvalue stability of spectral methods*, in Numerical Methods for Fluid Dynamics III, K. Morton and M. Bains, eds., Clarendon Press, Oxford, 1988, pp. 237–253.
- [25] J. VARAH, *Stability restrictions on second-order, three level finite difference schemes for parabolic equations*, SIAM J. Numer. Anal., 17 (1980), pp. 300–309.
- [26] R. VARGA, *Matrix Iterative Analysis*, Prentice-Hall, Englewood Cliffs, NJ, 1962.